Coastal Engineering 56 (2009) 23–31

Contents lists available at ScienceDirect

Coastal Engineering

journal homepage: www.elsevier.com/locate/coastaleng

On the application of a Boussinesq model to river flows including shocks

Emmanuel Mignot, Rodrigo Cienfuegos *

Departamento de Ingeniería Hidráulica y Ambiental, Pontificia Universidad Católica de Chile, Av. Vicuña Mackenna 4860, casilla 306, correo 221, Santiago, Chile

ARTICLE INFO

Article history:
Received 22 July 2007
Received in revised form 14 May 2008
Accepted 6 June 2008
Available online 14 July 2008

Keywords:
Boussinesq-type equations
Wave-breaking
Dam-break
Hydraulic jump
Absorbing-generating boundary condition

ABSTRACT

SERR-1D is a 4th-order finite volume 1D Boussinesq model including wave breaking energy dissipation through extra diffusive-like terms. This model has been primarily conceived to compute wave propagation in coastal areas and has been validated for breaking and non-breaking waves propagating over uneven bathymetries (Cienfuegos et al., 2005, 2006a, b, 2007). The present paper aims at investigating the ability of SERR-1D to simulate challenging fluvial hydraulic applications such as sudden gate operation in open channels generating short waves, dam-break flows and a steady hydraulic jump over a bump. The performance of the absorbing-generating boundary condition implemented in SERR-1D is first analysed in the context of fluvial applications where relatively short waves must be evacuated from the computational domain without producing spurious reflection. Next, by comparing numerical results to analytical and experimental dam-break test cases we show that the model is able to reproduce the overall features of these flows, but that additional care should be paid to the representation of energy dissipation and front speed in order to accurately represent bore dynamics.

© 2008 Elsevier B.V. All rights reserved.

1. Introduction

Many hydraulic and coastal engineering applications require an accurate prediction of wave propagation phenomena. Wave propagation over a beach, gate operation in natural or artificial channels, sudden failure of reservoir dams, constitute important examples. While most riverine applications can be usually tackled using a long wave approximation through the hydrostatic pressure distribution assumption, governing equations for engineering problems involving relatively short waves propagating over shallow waters must take into account the effect of strong free surface curvatures and vertical accelerations. In addition, a large amount of energy is dissipated in hydraulic jumps, bores or surf zone waves and it is expected that the chosen set of governing equations could be able to reproduce this phenomenon.

The dispersionless Saint–Venant (S–V) equations, widely used in riverine applications, are able to describe river flows and even non-linear broken wave dynamics as long as appropriate shock-capturing numerical techniques are employed (see Toro, 2001, for a comprehensive review). For instance, dam break propagation (e.g. Yang and Chang, 1993; Bradford and Sanders, 2002) or quasi-periodic bore propagation in the inner surf zone (e.g. Kobayashi et al., 1989; Bonneton, 2007) can be accurately computed using S–V equations. However, because of the hydrostatic assumption, the validity range of S–V equations is restricted to long wave propagation where $h_0/\lambda < 1/20$, h_0 being a characteristic water depth and λ a characteristic wave-length. Thus, short wave dynamics in shallow water should be described by non-hydrostatic theories such as KDV or Boussinesq-type (B–T) equations since they account for the combined effect of non-linearity and dispersion (see Whitham, 1974).

For practical riverine or coastal applications involving relatively short waves (say up to $h_0/\lambda < 1/2$) and breaking, a unified theory able to represent both, non-hydrostatic processes and non-linear shocks is required. Unfortunately, even if from a mathematical standpoint, B–T equations asymptotically tend to S–V equations as the ratio h_0/λ tend to zero, shock-wave solutions are not strictly supported by the former because of the mixed parabolic-hyperbolic nature of their governing partial differential equations. In this framework, the preferred approach consists in incorporating shock-wave energy dissipation in B–T equations through extra diffusive-like terms (see Kirby, 2003, for a recent review).

SERR-1D (Cienfuegos et al., 2005, 2006a, b, 2007) is a fully non-linear and weakly dispersive B–T model primarily developed to compute wave propagation in coastal areas. Wave-breaking energy dissipation is taken into account through extra terms, written both in mass and momentum conservation equations, carefully conceived in order to extract the amount of energy that would occur in shock waves. Moreover, the mathematical form of these terms ensures that mass and momentum are only locally redistributed below breakers thus preserving the overall budget for these quantities. This model has been calibrated and validated on breaking and non-breaking coastal waves propagating over uneven bottom bathymetries (Cienfuegos et al., 2005, 2006b, 2007) and we aim in the present paper at investigating its

* Corresponding author.
E-mail addresses: emmanuel.mignot@hmg.inpg.fr (E. Mignot), racienfu@ing.puc.cl (R. Cienfuegos).

0378-3839/$ – see front matter © 2008 Elsevier B.V. All rights reserved.
doi:10.1016/j.coastaleng.2008.06.007

ability to simulate riverine applications including shocks, traditionally solved using S–V equations.

In the present work, we evaluate SERR-1D predictions on several typical riverine applications, some of which include energy dissipation through shocks (dam-break flows and steady hydraulic jumps). These types of flows are successfully treated using shock-capturing S–V solvers, and rather than questioning this fact, we investigate here if a B–T model with breaking can reasonably be applied over the range of wave propagation $h_0/\lambda<1/2$, from relatively short waves to fairly long waves including energy dissipation by breaking. Similarly, important practical issues concerning the implementation of boundary conditions in applications involving short waves propagating under subcritical flow conditions are discussed. Indeed, the characteristic decomposition of equations at the boundary, usually employed in fluvial hydraulics, can produce spurious wave reflection for outward traveling short waves leading eventually to numerical instabilities and/or inaccuracies (e.g. Sanders, 2002). The use of an absorbing-generating wave-type boundary condition, also termed as "non-reflecting" boundary, which allows free surface perturbations to freely leave the computational domain is thus required.

The first part of the article is devoted to describe SERR-1D governing equations focusing on the wave-breaking model and the absorbing-generating boundary condition, while in the second part, several benchmark tests are used to evaluate model's ability to freely evacuate short waves from the computational domain and to reproduce riverine applications including shocks.

2. Description of SERR-1D

2.1. Governing equations and breaking model

Numerical computations are conducted in the following using the 4th-order finite volume Boussinesq model SERR-1D (Cienfuegos et al., 2005, 2006a, b, 2007). Model predictions are in good agreement with measured spatio-temporal wave evolution (amplitude, asymmetry and phase speed) for non-breaking waves in the dispersive range $h_0/\lambda<1/2$. With the inclusion of wave-breaking energy dissipation and bottom friction, mass and momentum conservation equations can be written in the following generic form,

$$\frac{\partial h}{\partial t}+\frac{\partial}{\partial x}(hu)-D_h=0, \tag{1}$$

$$\frac{\partial u}{\partial t}+\frac{1}{2}\frac{\partial u^2}{\partial x}+g\frac{\partial h}{\partial x}+\Gamma_d-\frac{1}{h}D_{hu}+\frac{\tau_b}{\rho h}=0, \tag{2}$$

where ρ is the water density, h is the water depth, u is the depth-averaged horizontal velocity, D_h and D_{hu} represent breaking-induced functions to be described later, Γ_d contains all the dispersive terms, τ_b is the bed shear stress and g is the gravitational acceleration. Here, variables x and t denote fixed space and time coordinates.

Breaking-induced energy dissipation mechanism is introduced through diffusive-like terms, D_h and D_{hu}, applied locally on the wave front over a segment l_r starting at the wave crest (see Fig. 1). These terms are activated when breaking is likely to occur and thus require an explicit breaking criterion to switch them on. Following the strategy proposed by Schaffer et al. (1993), breaking is triggered if the mean local wave front breaker angle Φ is greater than the critical value $\Phi_b=31°$ and once breaking has been initiated, extra terms are switched off when the local front slope value falls below $\Phi_0=8°$. These values have been calibrated on Ting and Kirby (1994) regular wave experiment by Cienfuegos et al. (2005, 2006b).

The mathematical form for D_h and D_{hu} is chosen in order to ensure that the overall mass and momentum budget is preserved, acting only as to locally redistribute these quantities under the breaker. This approach is based on ideas previously developed by Zelt (1991) and Kennedy et al. (2000) who introduced a similar diffusive term in the momentum conservation equation.

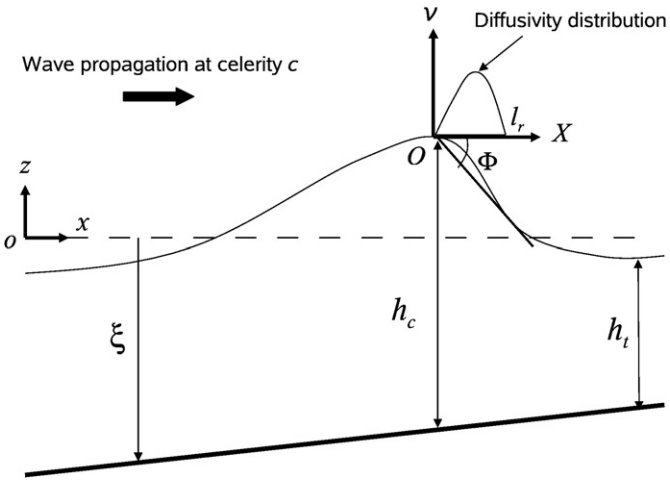

Fig. 1. Definition sketch for a breaking wave and related variables.

Breaking terms are thus written in the form,

$$D_h=\frac{\partial}{\partial x}\left(\nu_h\frac{\partial h}{\partial x}\right), \tag{3}$$

$$D_{hu}=\frac{\partial}{\partial x}\left(\nu_{hu}\frac{\partial hu}{\partial x}\right), \tag{4}$$

where ν_h and ν_{hu} are diffusivity functions which are expressed as (see Cienfuegos et al., 2005, 2006b),

$$\nu_h(X)=-\delta_h cd\,\exp\left(\frac{X}{l_r}-1\right)\left[\left(\frac{X}{l_r}-1\right)+\left(\frac{X}{l_r}-1\right)^2\right], \tag{5}$$

$$\nu_{hu}(X)=-\delta_{hu} cd\,\exp\left(\frac{X}{l_r}-1\right)\left[\left(\frac{X}{l_r}-1\right)+\left(\frac{X}{l_r}-1\right)^2\right], \tag{6}$$

where δ_h and δ_{hu} are constant scaling coefficients, c and d are characteristic velocity and length scales respectively, X is the horizontal coordinate attached to the wave crest in the moving frame of reference (O,X), and l_r is the extent over which breaking terms are active (see Fig. 1). The length scale d in the model is estimated as the local average between crest (h_c) and trough (h_t) water depths, and the velocity scale is computed as $c=\sqrt{gd}$. It is important to note that this particular functional form ensures an overall mass and momentum conservation over a breaking event because $\nu_h=\nu_{hu}=0$ at $X\le 0$ and $X\ge l_r$, being non-zero only on the forward face of the breaker. The extra mass diffusivity term in the mass conservation equation can be thought as the enhancement of local mass transfer by avalanching at the front face of the breaker, from the crest to the trough. This is in agreement with empirical observations and aims at traducing additional energy loss associated to vortical effects not taken into account by inviscid theories (see for instance Dutykh and Dias, 2007).

Numerical values for model parameters were calibrated on Ting and Kirby (1994) regular wave experiment by Cienfuegos et al. (2005, 2006b) producing,

$$\delta_{hu}=34 \tag{7}$$

$$\delta_h=3.4 \tag{8}$$

$$\frac{l_r}{d}=0.82. \tag{9}$$

These values are adopted hereafter.

Finally, for the estimation of the bed shear stress in Eq. (2) we use aquadratic friction model (Grant and Madsen, 1979),

$$\tau_b = \frac{1}{2} C_f \rho u|u| \tag{10}$$

with C_f an empirical non-dimensional roughness coefficient that can be related (for quasi-steady flows) to the well known Manning coefficient, n, through,

$$C_f = \frac{2g\, n^2}{h^{1/3}}. \tag{11}$$

2.2. Boundary conditions

At the present stage of development, three types of boundary conditions are implemented in SERR-1D: a moving shoreline boundary condition adapted from Lynett et al. (2002), a fully reflective wall boundary and an absorbing-generating boundary for subcritical flows allowing to prescribe incident waves while letting outward directed waves to freely leave the computational domain (Cienfuegos et al., 2007).

For riverine applications, we modify the absorbing-generating boundary condition in order to be able to prescribe flow discharge, q_b, at a given subcritical channel section. In addition, we take into account friction and non-uniform bathymetries at the boundary location. It is important to note that for subcritical flows, relatively short waves propagating through model boundaries must freely leave the domain without generating any spurious partial reflection thus effectively simulating an open boundary.

In order to write boundary conditions for subcritical flows it is useful to recast B–T equations in the following quasi-hyperbolic form (see Cienfuegos et al., 2007),

$$\frac{dR^+}{dt} = -g\,\xi_x - \frac{\tau_b}{\rho h} + O(\sigma^2) \quad \text{along} \quad \frac{dx}{dt} = u + \sqrt{gh} \tag{12}$$

$$\frac{dR^-}{dt} = -g\,\xi_x - \frac{\tau_b}{\rho h} + O(\sigma^2) \quad \text{along} \quad \frac{dx}{dt} = u - \sqrt{gh} \tag{13}$$

where $R^+ = u + 2\sqrt{gh}$ and $R^- = u - 2\sqrt{gh}$ are respectively positive and negative Riemann variables, ξ_x is the local bottom slope ($z=\xi$ is the local bottom elevation), and $\sigma = |\xi|/\lambda$ is the dispersive parameter with λ being the local wave-length. For S–V equations $\sigma^2 \ll 1$ while for the current B–T model, $\sigma^2 < 1/4$. Eqs. (12)–(13) are formally known as characteristic equations.

In classic hydraulics and for subcritical flows, one has to prescribe the value of either h or u at the boundary and the remaining variable is computed by solving the characteristic Eq. (12) or Eq. (13) carrying information from the interior domain (Cunge et al., 1980). This approach is best suited for control sections where the flow velocity (discharge) or the water depth are known at every time step. However, if relatively short waves propagate from the interior domain through an open end, both, the velocity and the water depth need to adjust themselves in order to allow flow perturbations to freely leave the domain. In this case, an absorbing-generating boundary condition has to be implemented.

The adopted strategy, for an incident wave field coming from the left in Fig. 2 into the area of interest, consists in assuming that the right-going Riemann variable, R^+, arriving at the boundary location A′ at $t+\Delta t/2$, can be computed using water depth and velocity values in the fictitious domain at location L. Assuming that the incoming field propagates with permanent form at celerity $c_0 = \sqrt{gh_0}$ (taking h_0 as the mean water depth at the domain boundary) the prescribed boundary value for water depth, $h_b(t)$, can be used to evaluate water depth at location L as $h_L = h_b(x_A + c_0\,\Delta t/2)$ where x_A is the spatial coordinate of the boundary. The velocity at L is then estimated as $u_L = c_0\,(h_L - h_0)/h_L$

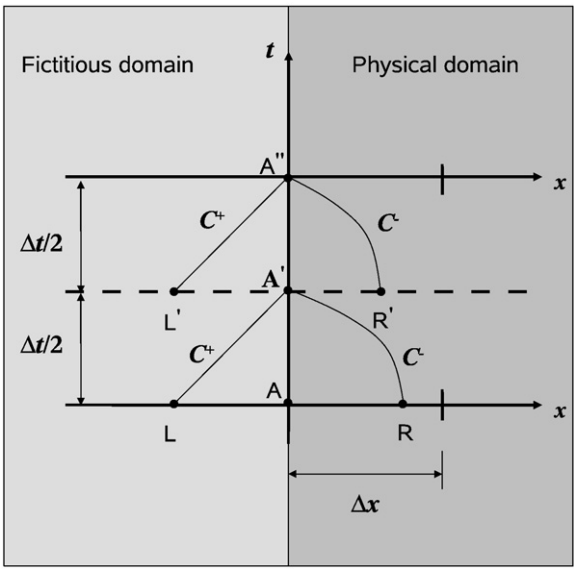

Fig. 2. Characteristic positive, C^+, and negative, C^-, curves in the x–t plane sketching the fictitious and physical domain decomposition strategy.

which follows from the permanent form assumption. This simple strategy then fixes the value of the incoming Riemann variable, which is evaluated as,

$$R_L^+ = u_L + 2\sqrt{gh_L}. \tag{14}$$

On the other hand, the left-going Riemann variable, R^-, arriving at the location A' at $t+\Delta t/2$, is computed once position, R, is determined by backward integration along the C^- trajectory. This is done by solving the non-linear equation by a standard Newton–Raphson strategy and linearly interpolating known water depth and velocity values in the physical domain at time t. The left-going Riemann variable is then evaluated at point R as,

$$R_R^- = u_R - 2\sqrt{gh_R}, \tag{15}$$

where u_R and h_R correspond to velocity and water depth at location R (linearly interpolated from known nodal values in the physical domain). Finally, boundary values for flow velocity, $u_{A'}$, and water depth, $h_{A'}$, at $t+\Delta t/2$ are computed from characteristic Eqs. (12)–(13) as,

$$u_{A'} = \frac{1}{2}(I_L + I_R), \tag{16}$$

$$h_{A'} = \frac{1}{16g}(I_L - I_R)^2, \tag{17}$$

where,

$$I_L = R_L^+ - \frac{\Delta t}{2}\left\{ g\,\xi_x + \frac{1}{\rho}\frac{\tau_b}{h} \right\}_L + O(\sigma^2 \Delta t), \tag{18}$$

$$I_R = R_R^- - \frac{\Delta t}{2}\left\{ g\,\xi_x + \frac{1}{\rho}\frac{\tau_b}{h} \right\}_R + O(\sigma^2 \Delta t). \tag{19}$$

Here $\{\}_R$ means that terms in bracket are evaluated at location R.

Since in SERR-1D, B–T equations are advanced in time through a Runge–Kutta time stepping, the numerical solution is evaluated twice at $t+\Delta t/2$ and twice at $t+\Delta t$. In the first step, which we just described, Eqs. (12)–(13) are numerically integrated between t and $t+\Delta t/2$ along characteristic trajectories using an explicit first order approximation for the time integral. In the second Runge-Kutta step, implicit numerical

time integration of Eqs. (12)–(13) can be performed with improved accuracy since estimates for u_A' and h_A' are now available. A similar procedure is employed, starting at $t+\Delta t/2$, for the third and fourth Runge-Kutta steps. Then, using partial estimates for water depth and velocity at each step finally provides boundary values at $t+\Delta t$ which preserve the 4th order accuracy of the scheme. This strategy produces an absorbing-generating boundary condition by allowing both, water depth and velocity, to adjust themselves taking into account incident and out-going wave fields. This will be demonstrated in subsequent sections.

For riverine applications, where an inflow discharge is instead prescribed, the strategy just described must be slightly modified. In this case we assume that, in the fictitious domain, the incoming discharge, q_b, and the associated water depth, h_b, are both known. Then the incoming Riemann variable at L is computed as,

$$R_L^+ = \frac{q_b}{h_b} + 2\sqrt{g h_b}, \tag{20}$$

and the out-going Riemann variable is computed as before.

It is worth noting that even if the absorbing-generating boundary condition just described is based on an incoming and outgoing wave decomposition similar to the one proposed by Van Dongeren and Svendsen (1997), the present approach does not rely on any small amplitude wave hypothesis (linearization), by only invoking a permanent form incident wave field assumption. Hence, highly non-linear waves could in principle be prescribed at the boundary and evacuated from the interior domain. Furthermore, the adopted four-stage strategy allows for higher accuracy thus reducing spurious reflection at the boundary for a given wave condition, grid resolution and time step. An alternative approach, where an absorbing-generating boundary condition is achieved in the context of a finite volume method, has been presented by Brocchini et al. (2001) using an implicit Riemann solver and without invoking a permanent form assumption.

3. Evaluation of SERR-1D on riverine applications

The objective of the present section is to test the capacities of SERR-1D when applied to complex river flow configurations focusing on i) the performance of the absorbing-generating boundary condition when relatively short waves need to be evacuated from the domain, and ii) the ability of the breaking-wave parameterization to reproduce energy dissipation through shocks. For all computations described in the following, model parameters are set to the values described in Section 2.1.

3.1. Sudden gate closure in a subcritical channel flow

The effectiveness of the implemented absorbing-generating boundary condition is first analyzed by applying SERR-1D to a typical engineering problem involving gate operation on a wide rectangular channel. As initial condition, a steady subcritical flow is considered within a frictionless semi-infinite horizontal channel conducting a volumetric discharge of $q_0=0.3$ m^2/s with a constant water depth $h_0=0.6$ m. At time $t=0$, a gate located at the downstream end of the channel is operated in order to linearly reduce the outflow discharge down to zero during a time interval $\Delta t_g=0.5$ s. The downstream flow rate is then immediately increased back to the initial value q_0 during an equivalent time interval Δt_g. This rapid gate operation produces highly non-linear and dispersive (short) waves that propagate upstream and eventually reach the inflow boundary.

In the situation described above, the traditional treatment of subcritical upstream boundary conditions in the framework of S–V equations consists in prescribing the discharge and computing the local water depth using the outward directed characteristic equation. However, this may produce spurious reflection at the boundary if short waves generated within the domain reach the upstream end. In order to avoid this unphysical behavior, computational domain would have to be large enough to ensure that perturbations do not have time to reach the inflow boundary during the calculation. On the contrary, implementing an absorbing-generating boundary condition may effectively produce an open end within the channel, allowing to reduce the extent of the computational domain. Concerning the downstream boundary condition, the given discharge evolution $q_d(t)$ at the gate is prescribed and the associated water depth is computed using the out-going characteristic equation as it is usually done in fluvial hydraulics. By doing so, we reproduce the rapid gate operation and generate relatively short waves traveling in the upstream direction.

In order to evaluate the implemented absorbing-generating upstream boundary, three different lengths for the computational domain are considered next.

- Case 1. the channel is infinitely long upstream from the gate and thus the computed flow is not influenced by the upstream boundary condition.
- Case 2. the channel is 25 m long with the absorbing-generating boundary condition implemented upstream. The incoming Riemann variable is computed using relation (20) taking $q_b=q_0$ and $h_b=h_0$.
- Case 3. the channel is 5 m long with the absorbing-generating boundary condition implemented upstream. The incoming Riemann variable is computed as in Case 2.

Water depths computed at a distance $D=20$ m from the gate using the infinite domain (Case 1) and the 25 m domain (Case 2) are compared in Fig. 3 while water depth evolution at $D=4$ m, using the infinite domain and the 5 m domain (Case 3), are compared in Fig. 4. Results show that the influence of the absorbing-generating boundary condition on the interior domain is very small since there are only minor differences between computed water depths at a fixed location using an infinite or a finite domain. Mild differences appear for Case 3 where small oscillations still remain even after the dispersive wave train should have left the domain ($t>18$ s). These oscillations originate as the traveling short waves reach the upstream boundary and are not fully absorbed. Then, they back-propagate towards the downstream end where they are fully reflected. However, it is important to note that the amplitude of these oscillations is much smaller than the amplitude of the waves created during the gate operation proving that the absorbing-generating boundary condition performs well even for highly non-linear waves. Hence, the implemented boundary condition acts as an open boundary since its relative location within the domain does not have much influence on computed results.

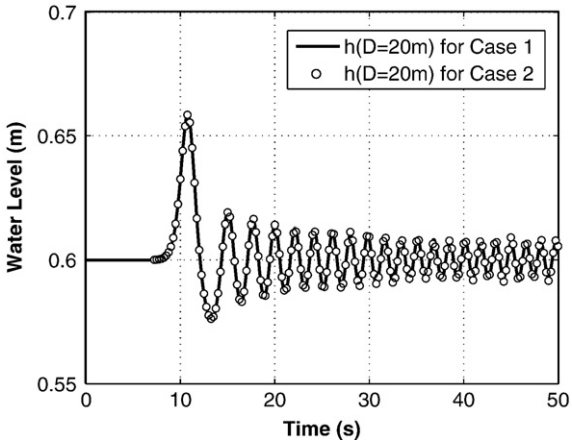

Fig. 3. Sudden gate closure in a channel. Comparison of computed water depths at a distance of 20 m from the gate (Cases 1 and 2).

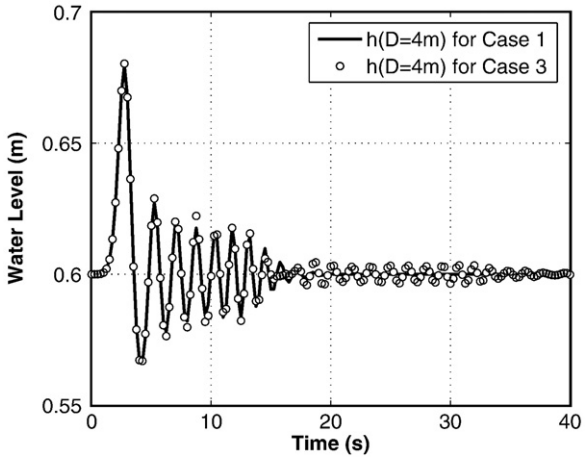

Fig. 4. Sudden gate closure in a channel. Comparison of computed water depths at a distance of 4 m from the gate (Cases 1 and 3).

It is worth noting that the characteristic wave-length in this example is of nearly $\lambda = 4.8$ m (based on linear theory), leading to a depth over length ratio $h_0/\!/ = 0.13$, a value which is far beyond the limit of application of S–V equations. Indeed, in the framework of S–V theory, these short waves will rapidly deform and eventually break because of non-linearity. On the contrary, in B–T equations, dispersive effects are counterbalanced by non-linearity thus resulting in propagating waves of more stable forms. It is worth emphasizing that dispersion is very strong in this example since the dispersive tail observed in Fig. 4 at location $D = 4$ m is widened in Fig. 3, which corresponds to the free surface evolution at location $D = 20$ m. Indeed, the number of individual waves has strongly increased between both locations, a feature that is typical of dispersive wave trains.

3.2. Dam-break flows

The dam break consists in a sudden removal of a gate which initially separates two flow regions at rest with different water levels. Various experimental dam-break flow configurations have been studied in the past, such as dam-break propagation over dry and wet, fixed or loose beds. Depending on the initial conditions, two well-known situations arise for a fixed bed dam break: i) over a dry bottom, two rarefaction waves appear, the free surface profile is smooth at all times and no breaking occurs, and ii) over an initially wet bed, a rarefaction wave develops on the high initial water depth region and a shock appears on the low water depth region immediately after the dam removal. In the framework of S–V equations, analytical solutions for the evolution of water surface profile and wave-front propagation exist for both cases.

Five dam break experimental configurations were selected from the literature (Table 1). For the simulation of Leal 01 and Leal 02 dam break experiments over horizontal bottoms (see Leal et al., 2006, for detailed description), we focus on the analysis of the wave front dynamics, and the free surface evolution. The experimental set-ups of Aureli et al 01 and Aureli et al 02 (from Aureli et al. (2000), but originally published in Belicchi (1997)) aim at verifying the ability of the numerical model to simulate the attenuation of the wave-front on an adverse slope. Finally, Aureli et al 03 experimental configuration provides an opportunity to study the wave front propagation over rough beds. It is worth noting that these experimental set-ups also permit to check the accuracy of the moving shoreline boundary condition implemented in SERR-1D.

Leal et al. (2006) experiment consists in a 20.05 m long and 0.5 m wide horizontal channel with a 10.08 m long reservoir closed by a gate. The gate, located at $x = 10.08$ m ($x = 0$ being fixed at the upstream end of the reservoir) is instantaneously removed using counter-weight mechanism (Leal et al., 2002). Five pressure transducers are used to measure the water depth evolution, both in the reservoir and along the channel.

Table 1
Experimental dam break tests with h_1 and h_2 the upstream and downstream initial water depth and x being the horizontal coordinate ($x = 0$ is fixed at the upstream end of the channel)

Test ID	h_1 (m)	h_2 (m)	Bed topography	Gauge locations x(m)
Leal_01	0.405	0.0	Horizontal	8.5, 10.2, 11, 13, 17
Leal_02	0.405	0.049	Horizontal	8.5, 11, 12, 13, 15
Aureli et al 01	0.25	0.0	Horiz.+adverse slope	3.4, 4.5
Aureli et al 02	0.25	0.045	Horiz.+adverse slope	3.4, 4.5

On the other hand, Aureli et al. (2000) experimental flume is 7 m long and 0.5 m wide, with a 2.25 m long horizontal reservoir and a 10% adverse slope starting at $x = 3.4$ m ($x = 0$ m being fixed at the upstream end of the reservoir). A gate opening procedure similar to the one described above is applied. The free surface evolution in the horizontal channel at section $x = 3.4$ m and in the adverse slope at section $x = 4.5$ m are captured using video recording.

In all computations, initial conditions correspond to those described in the original papers, i.e. two different water depth regions at rest as given in Table 1. When the dam-break wave propagates over an initially wet bottom, wall boundary conditions are implemented at both channel ends. For initially dry bottoms, the moving-shoreline boundary condition is employed to track the dry-wet interface while a wall boundary is considered at the upstream end. Whenever the breaking criterion is reached, the dissipation terms in Eqs. (1) and (2) are activated leading to a local energy dissipation in the vicinity of the wave front.

3.2.1. Dam-break over horizontal bottom

For initially dry bottoms, no breaking occurs in the experiment, leading to a smooth free surface evolution in time. Correspondingly, in the numerical simulation, the breaking criterion is never reached, due to the low front face slope. The comparison of numerical calculation of Leal 01 case with Ritter (1892) solution depicted in Fig. 5 shows that model predictions are quite close to the S–V exact solution. Similarly, Fig. 6 shows a fairly good agreement between computed free surface evolution and experimental measurements except at the gauge located very close to the dam ($x = 10.2$ m) where computed water depth profile evolves faster than the measured one. The discrepancy at the initial stage of the flow may be attributed to differences between the numerical and experimental dam removal mechanism, since the latter is not instantaneous as in the numerical model. Anyhow, computed results are in

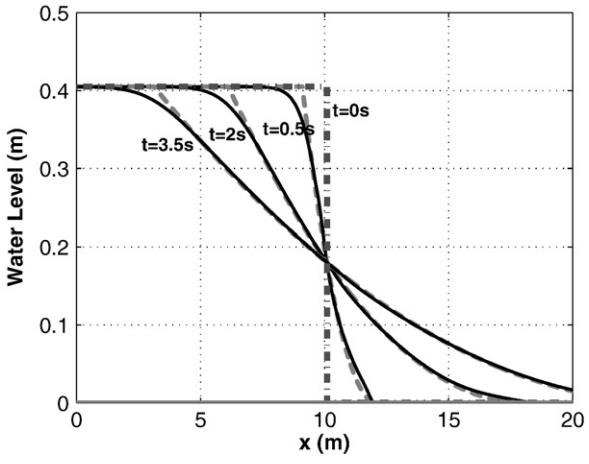

Fig. 5. Case Leal 01 dam break over dry bed (from Leal et al. (2006)). Comparison of computed water depth profiles (full line), using $\Delta x = 0.05$ m and $\Delta t = 2$ ms, and Ritter (1892) analytical solution (dash line) at different times after dam removal.

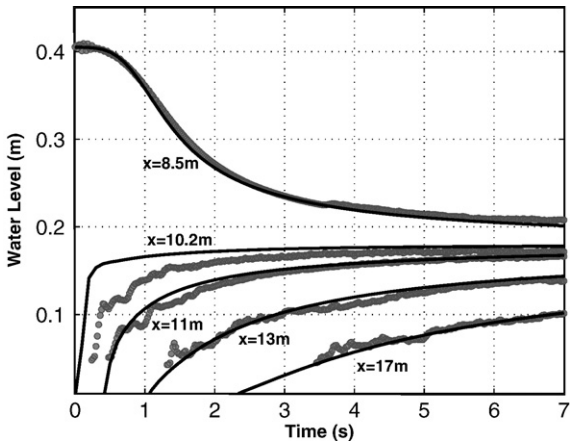

Fig. 6. Case Leal 01 dam break over dry bed (from Leal et al. (2006)). Comparison between experimental (symbols) and computed (solid line) free surface time series at different gauge locations using $\Delta x = 0.05$ m and $\Delta t = 2$ ms.

good agreement with experiments and are useful to demonstrate the ability of the moving front boundary condition to track the wet–dry interface. However, it should be noted that the time step must remain small in order to obtain accurate predictions, with a typical Courant number, based on the initial water depth, being less than 0.1.

On the other hand, over the initially wet bottom, the wave front steepens as the wave front propagates downstream. Numerically, the breaking criterion is reached and the breaking model is activated after $t = 0.5$ s and it remains active until the end of the computation. When comparing numerical results to Stoker (1957) solution in Fig. 7, it appears that overall water depth evolution on both sides of the dam is reasonably predicted but an overestimation of the computed water depth and an underestimation of the front speed are observed in the downstream region. The latter could be attributed to a slight underestimation of energy dissipation in the shock wave. Even if for the experimental case depicted in Fig. 8, numerical predictions of water depths in the downstream region are in better agreement, they are still over predicted. Similarly, after the initial stage of bore propagation, where the computed front appears before the measured one probably for the same reason discussed before, the underestimation of the wave-front celerity is confirmed for subsequent time stacks. We recall that the breaking model is run with a set of parameters that have been calibrated on a rather different set-up where regular waves broke on a beach of constant slope. Thus, a retuning of model parameters could be required in order to accurately describe present applications.

3.2.2. Dam break wave over an adverse slope

For the dam release over the initially dry bed (Aureli_01 case), a rarefaction wave propagates first over the horizontal bottom until reaching the adverse slope at $x = 4.5$ m. From this location, the wave front climbs up the slope (run-up), reaches a maximum elevation and finally, runs-down. The wave front velocity decreases rapidly during the run-up phase and once the maximum elevation is reached a strong back-swash develops which eventually breaks at the toe of the slope. A second wave then propagates from this location back into the reservoir. The comparison between numerical results and experimental data presented in Fig. 9 for two wave gauges located at the toe of the slope ($x = 3.4$ m) and in the adverse slope ($x = 4.5$ m) shows that the wave celerity and the wave front profile are accurately reproduced. Thus, the run-up and run-down process of a dam-break wave propagating over an adverse slope are predicted in good agreement with experimental observations. Moreover, the model succeeds in producing the secondary wave front that propagates back to the reservoir. However, it is important to note that the breaking model was only active during a short period in the rushdown stage, and this might explain why model performance is better than in the previous case. Nevertheless, this application is useful to illustrate the ability of the B–T model to deal with wave motions that are traditionally tackled under the hydrostatic assumption.

When the dam release is performed over an initially wet bed (Aureli 02 case), a shock wave is created and propagates over the horizontal bed into the adverse slope. When reaching the shoreline at $x \approx 3.8$ m, the wave front then climbs up over a dry bed and the run-up process corresponds then to a Ritter (1892)'s rarefaction wave running up an adverse slope. Consequently, the shock wave "dies" at the shoreline. Finally, at the end of the run-up, the run-down initiates as a rapid back-swash. For the numerical computation, the breaking criterion is reached soon after the front starts propagating over the initially wet horizontal channel (as for Leal 02 case) and it stops just before reaching the shoreline. This results demonstrates that the breaking criterion succeeds in predicting breaking initiation and cessation for this flow configuration. Similarly, the water depth evolution both, at the toe of the slope ($x = 3.4$ m) and over the adverse slope ($x = 4.5$ m), are accurately predicted as observed in Fig. 10. However, small oscillations of the water surface at $x = 3.4$ m, that are not clearly observed experimentally, appear behind the wave front. The B–T succeeds in reproducing these type of flow configuration, but

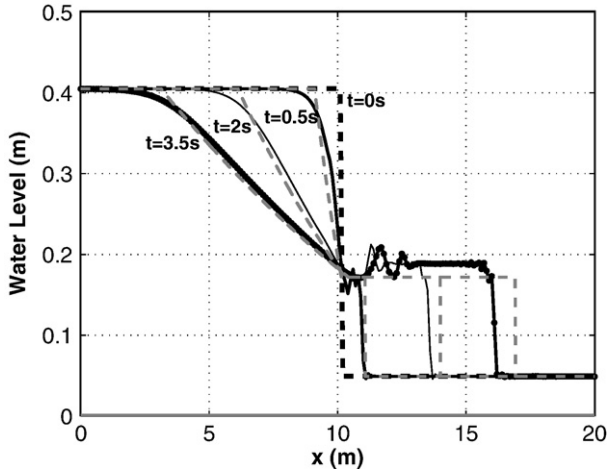

Fig. 7. Case Leal 02 dam break over wet bed (from Leal et al. (2002)). Comparison of numerical model (full line), using $\Delta x = 0.05$ m and $\Delta t = 12.5$ ms, and free surface profiles of Stoker (1957) solution (dash line) at different times after dam removal.

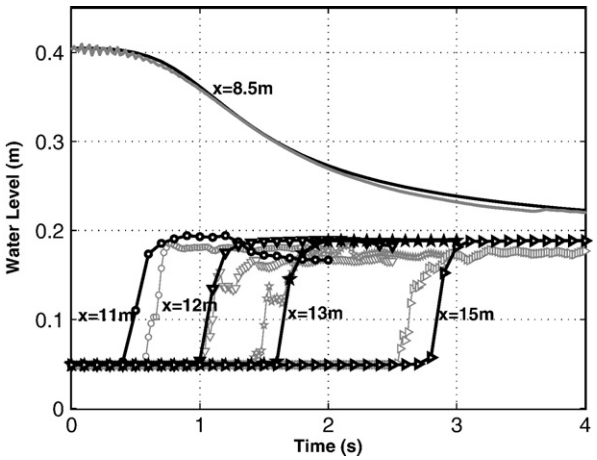

Fig. 8. Case Leal 02 dam break over wet bed (from Leal et al. (2002)). Comparison between experimental (grey) and computed (bold black) free surface time series at different gauge locations using $\Delta x = 0.05$ m and $\Delta t = 12.5$ ms.

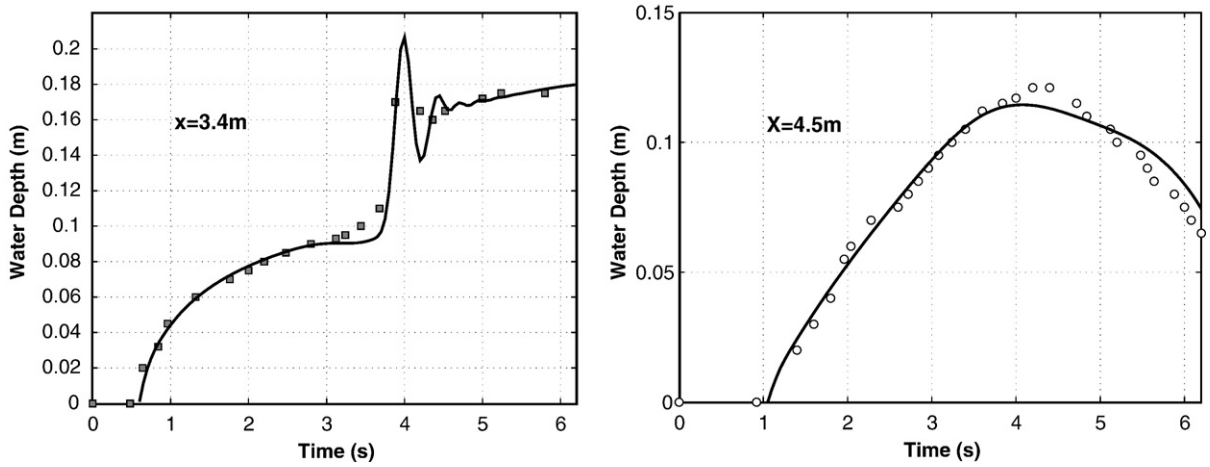

Fig. 9. Case Aureli 01 dam break over a dry bed (from Aureli et al. (2000)). Comparison between experimental (symbols) and numerical (full line) free surface time series at different wave gauges using Δx=0.05 m and Δt=2.6 ms.

we note that the breaking model is only active in this case on the first stage of propagation of the dam-break wave.

3.3. Steady hydraulic jumps

Hydraulic jumps are one of the most challenging riverine flow patterns to be reproduced by numerical models. An accurate prediction of hydraulic jump location, geometry and sequent water depths, requires a specific numerical treatment in order to capture flow discontinuities across a shock using S–V equations (e.g. Toro, 2001). In the framework of B–T equations, additional difficulties arise since dispersive terms introduce higher order derivatives in space and time. Obtaining a steady state solution retaining all dispersive terms in a fully non-linear B–T model is not trivial owing to high frequency oscillations that may arise during the initial unsteady flow adjustment. These high frequency perturbations may propagate across the jump and reach the downstream boundary. It is thus crucial to implement absorbing-generating boundary conditions in order to avoid spurious reflection. Several hydraulic jump computations performed using B–T equations can be found in the literature (e.g. Gharangik and Chaudhry, 1991; Soares-Frazao and Zech, 2002; Rao, 2002). However, these authors have mostly used low-order B–T models and often temporal derivatives in dispersive terms were disregarded in order to avoid high frequency oscillations leading eventually to numerical instabilities.

In the following application, numerical results are obtained using the complete set of fully non-linear B–T equations included in SERR-1D. It is worth noting that the chosen hydraulic jump test case provide an opportunity to further validate the breaking-wave parameterization included in SERR-1D.

3.3.1. Hydraulic jump over a bar

Madsen et al. (2005) investigated the accuracy and stability of a S–V numerical code by comparing its predictions against an analytical steady state solution available for a hydraulic jump generated over a frictionless submerged bar. The bathymetry of the test case is a horizontal bottom with a bump superimposed to it. The equation for the bump reads,

$$B(x) = 0.2\left(1-\left(\frac{x-15}{4}\right)^2\right) \quad 11 \le x \le 19 \tag{21}$$

where $B(x)$ is the bottom level and x the horizontal coordinate (see Fig. 11). Subcritical flow conditions occur at both ends of the flume with an upstream water depth h_1=0.5 m and a downstream water depth h_2=0.48 m. Flow discharge per unit width is q_0=0.3 m^2/s. The simulation of this test case using SERR-1D is described hereafter.

The numerical computation is initialized assuming a constant flow discharge, q_0 , and a constant water depth equal to the downstream boundary depth, h_2 , over the whole domain. Since both boundary sections are subcritical, absorbing-generating boundary conditions are considered there. Riemann variables for left and right fictitious domains are computed fixing the constant discharge per unit width at q_0, the upstream water depth at h_1, and the downstream water depth at h_2.

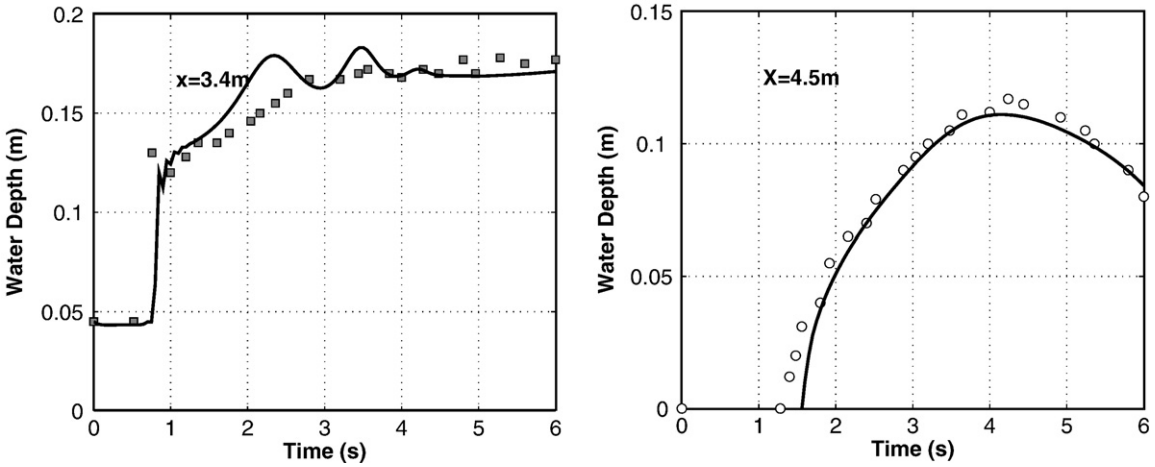

Fig. 10. Case Aureli 02 dam break over a dry bed (same caption as in Fig. 9) using Δx=0.05 m and Δt=16 ms for numerical computation.

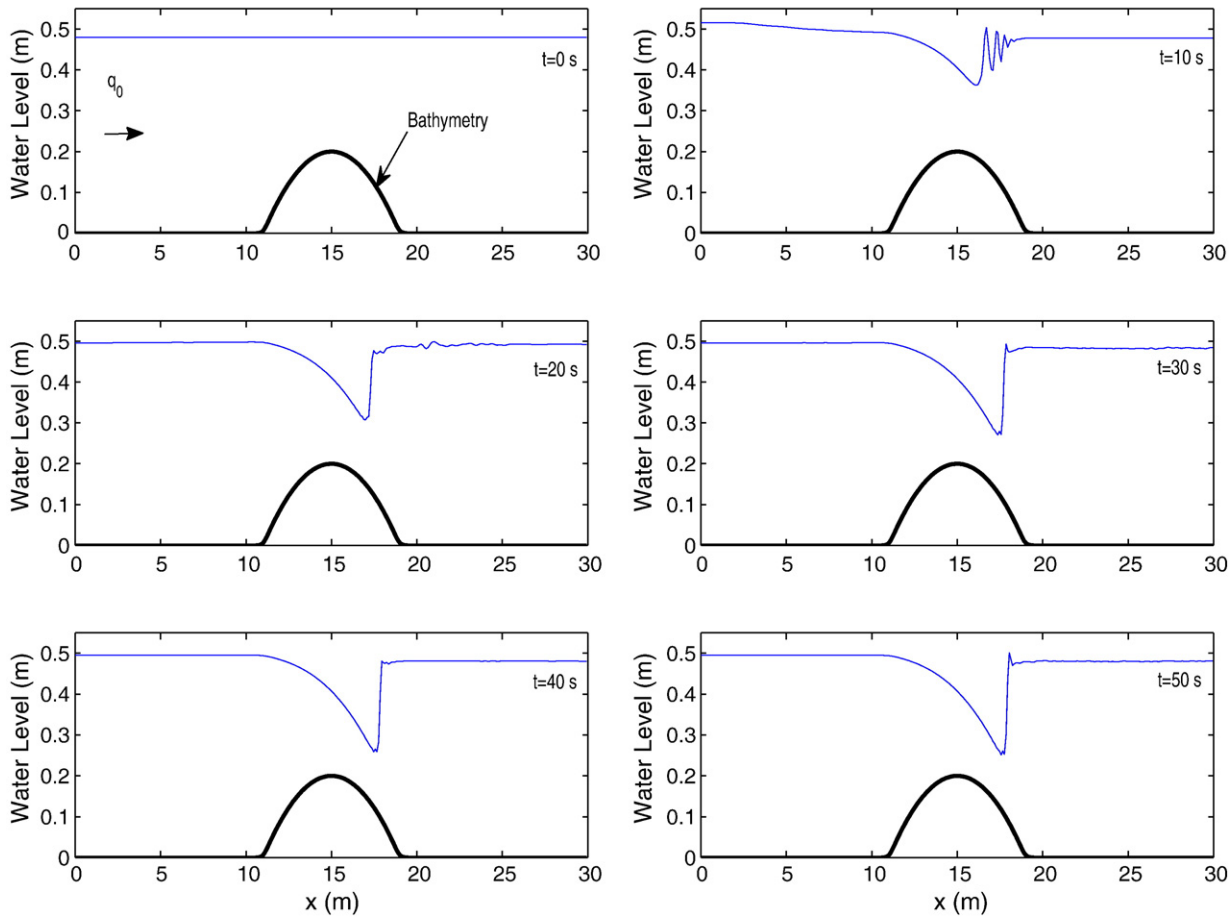

Fig. 11. Hydraulic jump over a frictionless bar. Computed free surface profiles at different times using $\Delta x = 0.1$ m and $\Delta t = 22$ ms.

Soon after the initialization of the numerical computation, the flow accelerates over the downstream slope of the bar and a slight increase in water depth is observed over the upstream part of the flume. During the unsteady flow adjustment, a dispersive wave train is created (see the water depth profile at $t = 10$ s in Fig. 11) but rapidly merges into a single wave front. This feature is a signature of non-hydrostatic effects included in B–T equations but are not present when using S–V models. After the bar, the flow remains sub-critical constrained by the downstream boundary condition and a hydraulic jump is created over the downstream slope of the bump. The breaking criterion is reached in the model soon after $t = 12$ s, where the breaking model starts dissipating energy and a hydraulic jump is produced. The jump is first located just downstream of the top of the bump but moves downstream until being stabilized after nearly 40 s in the middle of the downstream slope of the bar (see Fig. 12). It is interesting to note that at early stages of computation, water depths at the upstream and downstream boundaries oscillate around prescribed values thus adjusting themselves in order to evacuate transient waves generated inside the domain. When the steady state is reached, imposed boundary values for water depths are satisfied thus confirming that the implemented absorbing-generating boundary condition is well suited for this type of flow applications.

In Fig. 12, we show the computed free surface profile and the analytical solution available for S–V equations. It is seen that the computed location of the hydraulic jump is downstream from the analytical S–V solution. Nevertheless, water levels upstream and downstream of the jump are correctly predicted by the model thus suggesting that the overall energy dissipated across the shock agrees with the one produced by S–V equations.

Regarding the differences in jump location, we do not have a clear explanation since, to the authors knowledge, this is the first study where a B–T model is applied to this benchmark test. However, we feel that either it might be due to an incorrect phase speed estimation, or to the fact that the analytical solution for S–V equations does not exactly match the Boussinesq solution. Regarding the latter, we must recall that the fully non-linear set of B–T equations implemented in SERR-1D contains additional terms which account for dispersive effects. Some of these extra terms contain partial derivatives of the bottom profile (see Cienfuegos et al., 2006a) and may explain some of the observed discrepancies specially over the bump where these terms are active.

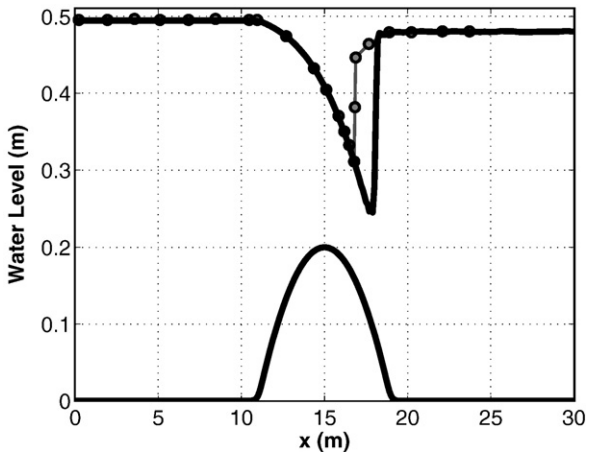

Fig. 12. Hydraulic jump over a frictionless bar. Computed steady state free surface profile (plain line) compared to Saint–Venant analytical solution (symbols).

Further investigation is required in order to elucidate what is the main source of discrepancy.

4. Conclusion

The present article has been devoted to investigate the ability of SERR-1D, a fully non-linear B–T model including breaking dissipation, to reproduce some important river flow patterns. The accuracy of a subcritical absorbing-generating boundary condition intended to effectively mimic open channel ends was first investigated in Section 3.1 using a numerical example of a sudden gate operation within a wide channel. It has been successfully demonstrated that using a characteristic decomposition and a fictitious domain to write inward Riemann variables, it is possible to simulate an open boundary and to evacuate relatively short waves which are within the dispersive validity range of B–T equations.

In Sections 3.2 and 3.3, SERR-1D was applied to riverine flows such as dam break propagation over horizontal and sloping bottoms and a steady hydraulic jump produced over an uneven bathymetry. Numerical results were compared to analytical solutions for S–V equations and experimental measurements. Test cases were specifically chosen in order to evaluate the performance of the breaking-wave parameterization implemented in SERR-1D in situations which differ from the coastal framework where the model was originally derived and calibrated. Comparisons performed between numerical, experimental and analytical results demonstrate that the B–T model succeeds in reproducing overall wave front dynamics but potential drawbacks concerning the viscous-like breaking model implemented in SERR-1D were highlighted. Whereas dam break flows over horizontal dry bottoms and over a sloping bathymetry were accurately predicted by the B–T model, a slight overestimation of water depths and an underestimation of wave front celerity have been observed for bore propagation in dam break experiments over horizontal wet bottoms. The latter suggests that the numerical values for breaking model parameters, calibrated on regular wave experiments, should be re-analysed in order to correctly reproduce these type of river flows. Nevertheless, it has not been clearly elucidated in the present study if these discrepancies could be solely attributed to parameter values or to the intrinsic nature of the breaking model. This issue should be further investigated in order to assess the general applicability of the breaking model to shock waves in river flows.

In summary, SERR-1D can in principle be applied to 1D riverine applications where S–V equations are traditionally employed since the main features of complex river flow patterns were reasonably predicted. The latter confirms the largest range of application of B–T equations and their potential use in riverine computations. However, additional care should be paid to the representation of energy dissipation in shocks in order to provide a powerful hydrodynamic model able to describe a large range of flow configurations where the combined effect of non-linearity, dispersion and breaking has to be taken into account.

Acknowledgments

The authors wish to thank the Escuela de Ingeniería of the Pontificia Universidad Católica de Chile (PUC) for the post-doctoral fellowship awarded to Emmanuel Mignot. The financial support of the Fondecyt program, through the grant number 11060312, is also gratefully acknowledged. We also thank professors F. Aureli, J. Leal, A. Gharangik, P. Madsen and associate authors for sharing their experimental data.

References

Aureli, F., Mignosa, P., Tomirotti, M., 2000. Numerical simulation and experimental verification of dam-break flows with shocks. J. Hydraul. Res. 38 (3), 197–206.
Belicchi, M., 1997. Modellazione fisica e matematica dei denomeni di moto vario conseguenti al collasso di opera di ritenuta. PhD Thesis (in Italian), Universita degli Studi di Parma, Italy.
Bonneton, P., 2007. Modelling of periodic wave transformation in the inner surf zone. Ocean Eng. 34, 1459–1471.
Bradford, S., Sanders, B., 2002. Finite-volume model for shallow-water flooding of arbitrary topography. J. Hydraul. Eng. 128 (3), 289–298.
Brocchini, M., Bernetti, R., Mancinelli, A., Albertini, G., 2001. An efficient solver for nearshore flows based on the WAF method. Coast. Eng. 43, 105–129.
Cienfuegos, R., Barthelemy, E., Bonneton, P., 2005. A new wave-breaking parametrization for Boussinesq-type equations. 5th Int. Symp. Oc. Wave Meas. Anal. Madrid, Spain.
Cienfuegos, R., Barthelemy, E., Bonneton, P., 2006a. A fourth order compact finite volume scheme for fully nonlinear and weakly dispersive Boussinesq-type equations. Part I: model development and analysis. Int. J. Numer. Methods Fluids 51 (11), 1217–1253.
Cienfuegos, R., Barthelemy, E., Bonneton, P., 2006b. Nonlinear surf zone wave properties as estimated from boussinesq modelling: random waves and complex bathymetries. 30th Int. Conf. Coastal. Eng. San Diego, USA, pp. 360–371.
Cienfuegos, R., Barthelemy, E., Bonneton, P., 2007. A fourth order compact finite volume scheme for fully nonlinear and weakly dispersive Boussinesq-type equations. Part II: boundary conditions and validation. Int. J. Numer. Methods Fluids 53 (9), 1423–1455.
Cunge, J., Holly, F., Verwey, A., 1980. Practical Aspects of Computational River Hydraulics. Pitman Publishing Limited, London. reprinted by Iowa Institute of Hydraulic Research.
Dutykh, D., Dias, F., 2007. Viscous potential free-surface flows in a fluid layer of finite depth. C. R. Acad. Sci. Paris, Ser. I 345, 113–118.
Gharangik, A., Chaudhry, M., 1991. Numerical simulation of hydraulic jump. J. Hydraul. Eng. 117 (9), 1195–1211.
Grant, W., Madsen, O., 1979. Combined wave and current interaction with a rough bottom. J. Geophys. Res. 84, 1797–1808.
Kennedy, A., Chen, Q., Kirby, J., Dalrymple, R., 2000. Boussinesq modeling of wave transformation, breaking and runup. I: 1D. J. Waterw. Port Coast. Occean Eng. 126 (1), 39–48.
Kirby, J., 2003. Boussinesq models and applications to nearshore wave propagation, surfzone processes and wave-induced currents. In: Lakhan, V. (Ed.), Advances in Coastal Modelling. Elsevier, pp. 1–41.
Kobayashi, N., De Silva, G., Watson, K., 1989. Wave transformation and swash oscillation on gentle and steep slopes. J. Geophys. Res. 94, 951–966.
Leal, J., Ferreira, R., Cardoso, A., 2002. Dam-break waves on movable bed. In: Bousmar Zech (Ed.), Proceeding River Flow 2002. Balkema, Rotterdam, The Netherlands, pp. 981–990. 2. San Diego, USA.
Leal, J., Ferreira, R., Cardoso, A., 2006. Dam-break wave-front celerity. J. Hydraul. Eng. 132 (1), 69–76.
Lynett, P., Wu, T., Liu, P., 2002. Modeling wave runup with depth-integrated equations. Coast. Eng. 46, 89–107.
Madsen, P., Simonsen, H., Pan, C., 2005. Numerical simulation of tidal bores and hydraulic jumps. Coast. Eng. 52, 409–433.
Rao, P., 2002. Contribution of Boussinesq pressure and bottom roughness terms for open channel flows with shocks. Appl. Math. Comput. 133, 581–590.
Ritter, A., 1892. Die fortpflanzung de wasserwellen. Zeitschrift Verein Deutscher Ingenieure (in German) 36 (33), 947–954.
Sanders, B., 2002. Non-reflecting boundary flux function for finite volume shallow-water models. Adv. Water Resour. 25, 195–202.
Schaffer, H., Madsen, P., Deigaard, R., 1993. A Boussinesq model for waves breaking in shallow water. Coast. Eng. 20, 185–202.
Soares-Frazao, S., Zech, Y., 2002. Undular bores and secondary waves — experiments and hybrid finite-volume modeling. J. Hydraul. Res. 40 (1), 33–43.
Stoker, J., 1957. Water waves: the mathematical theory with applications. Wiley-Interscience, New York.
Ting, F., Kirby, J., 1994. Observation of undertow and turbulence in a laboratory surf zone. Coast. Eng. 24, 51–80.
Toro, E., 2001. Shock-Capturing Methods for Free-Surface Flows, 1st Edition. John Wiley, New York.
Van Dongeren, A., Svendsen, I., 1997. Absorbing-generating boundary conditions for shallow water models. J. Waterw. Port Coast. Ocean Eng. 123 (6), 303–313.
Whitham, G., 1974. Linear and Nonlinear Waves, 1st Edition. Wiley Inter- Science.
Yang, J., Chang, S., 1993. Computations of free surface flows. I: one-dimensional dam-break flow. J. Hydraul. Res. 31 (1), 19–34.
Zelt, J., 1991. The run-up of nonbreaking and breaking solitary waves. Coast. Eng. 15, 205–246.